Supporting Information

Broadband multimodal THz waveguides for efficient transfer of high-power radiation in space-confined conditions

Anatoly R. Melnikov[a,b,c,*], Arkady A. Samsonenko[b,c], Yaroslav V. Getmanov[c,d], Oleg A. Shevchenko[d], Darya A. Shevchenko[d], Alexander A. Stepanov[a], Matvey V. Fedin[b,c], Maxim A. Yurkin[a,c], Sergey L. Veber[b,c,*]

[a] Voevodsky Institute of Chemical Kinetics and Combustion of the Siberian Branch of the Russian Academy of Sciences, 3, Institutskaya Str., Novosibirsk 630090, Russia
[b] International Tomography Center of the Siberian Branch of the Russian Academy of Sciences, 3a, Institutskaya Str., Novosibirsk 630090, Russia
[c] Novosibirsk State University, 1, Pirogova Str., Novosibirsk 630090, Russia
[d] Budker Institute of Nuclear Physics of the Siberian Branch of the Russian Academy of Sciences, 11, Acad. Lavrentieva Ave., Novosibirsk 630090, Russia

[*] Corresponding authors: anatoly.melnikov@tomo.nsc.ru; sergey.veber@tomo.nsc.ru

Contents

A. Procedure of the waveguide silvering

1. Surface cleaning

The surface of the unsilvered quartz tube was cleaned using the following procedure:

1. A freshly prepared concentrated solution of sodium hydroxide was poured into the tube for about 10 minutes. After that, the inner surface of the tube was thoroughly washed for about 5 minutes with a brush attached to a mechanical stirrer operating at about 300 rpm. Then the tube was rinsed with plenty of running water.
2. Concentrated hydrofluoric acid was poured into the tube for about 5 minutes. Next the tube was rinsed with plenty of running water.
3. Point 1 was repeated once more.
4. The tube was filled with a freshly prepared chromic-sulphuric acid mixture for about 10 minutes and then rinsed with plenty of running water.
5. Finally, the clean quartz tube was rinsed four times with distilled water.

2. Silver mirror reaction

To perform the silver mirror reaction, aqueous solutions of diamminesilver(I) hydroxide and glucose was freshly prepared for each iteration. All proportions are given for quartz tube 56 cm long and 6 mm inner diameter.

$[Ag(NH_3)_2]OH$:

55 mg of silver nitrate was dissolved in 2.2 ml of distilled water. Then, a concentrated solution of ammonia in water was added dropwise to it until the precipitated silver(I) oxide was dissolved. To the resulting clear solution was added 1.5 ml of 3% sodium hydroxide, the precipitate that formed was again dissolved by adding a concentrated ammonia solution dropwise. At the end, the solution was diluted with distilled water to 17 ml.

Glucose:

37 µl of a 40% glucose solution in water was diluted with 1 ml of distilled water, after which 3 drops of ethyl alcohol were added to the solution.

The silvering procedure was the following:

1. Freshly prepared aqueous solutions of diamminesilver(I) hydroxide and glucose were mixed and poured into a quartz tube for 2.30 minutes, counting from the moment the tube was filled. During the course of the reaction, silver was precipitated on the tube wall. After 2.30 minutes, the reagents were removed, and the tube was rinsed with distilled water one time.
2. Point 1 was repeated four to five times until the silver layer on the walls became opaque, which was checked with a flashlight.
3. Silvered waveguide was rinsed with distilled water, diluted ammonia solution, distilled water, and ethanol in the specified order. At the end, the waveguide was dried by dry nitrogen.

B. Spectra of radiation used for the waveguide performance study

Spectra of radiation used at the first and second FEL were measured using a modernized MDR-23 monochromator (Lomo Photonica, Russia) and MG-33 pirosensor (Vostok, Russia) installed on a support that is moved horizontally by a stepper motor controlled by a computer [1]. At the third FEL, radiation spectrum was measured by Fourier-transform infrared spectrometer Vertex 70v (Bruker Optics, Germany). The spectra are shown in Figs. S1-S4.

1. First FEL, 45.5 cm^{-1}

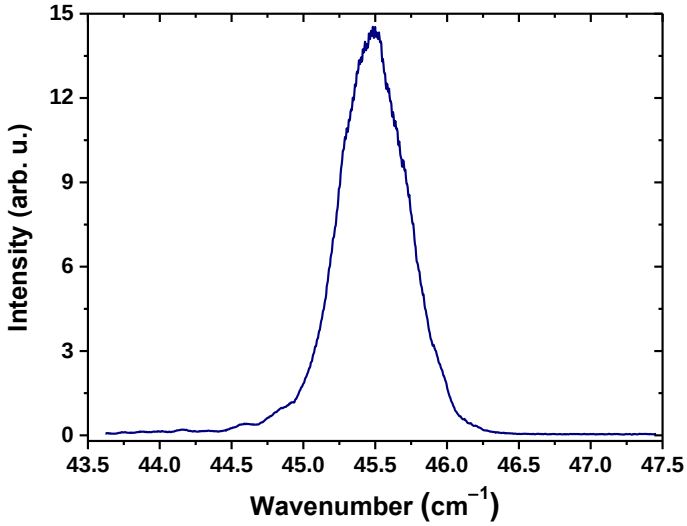

Fig. S1. Spectrum of radiation used for the performance study of the waveguides at 45.5 cm^{-1}. This energy is in the range of the first free electron laser (FEL) of the Novosibirsk free electron laser facility (NovoFEL).

2. First FEL, 77 cm^{-1}

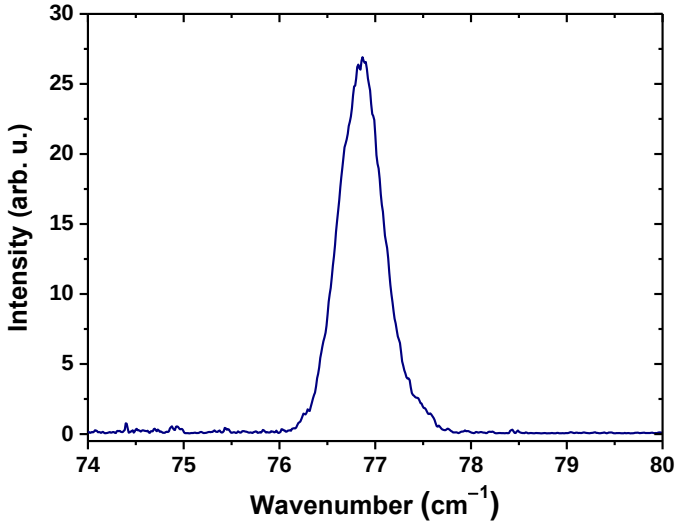

Fig. S2. Spectrum of radiation used for the performance study of the waveguides at 77 cm^{-1}. This energy is in the range of the first free electron laser (FEL) of the Novosibirsk free electron laser facility (NovoFEL).

3. Second FEL, 183 cm^{-1}

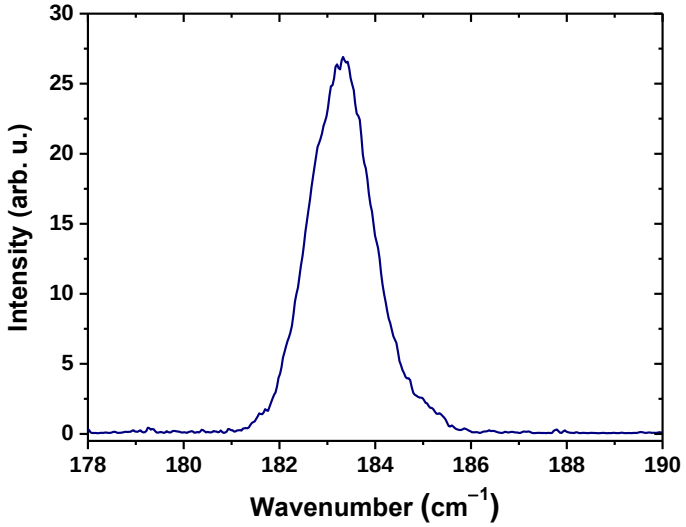

Fig. S3. Spectrum of radiation used for the performance study of the waveguides at 183 cm^{-1}. This energy is in the range of the second free electron laser (FEL) of the Novosibirsk free electron laser facility (NovoFEL).

4. Third FEL, 1118 cm^{-1}

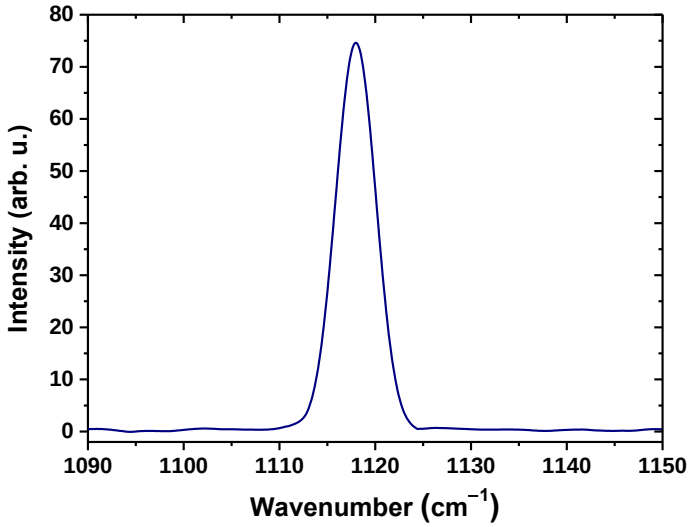

Fig. S4. Spectrum of radiation used for the performance study of the waveguides at 1118 cm^{-1}. This energy is in the range of the third free electron laser (FEL) of the Novosibirsk free electron laser facility (NovoFEL).

C. Additional modeling details

1. Transmittance and surface impedance

If the wavelength in the metal ($\delta \sim c/(\omega\sqrt{\varepsilon\mu})$, where c is the speed of light in vacuum, ω is angular frequency of radiation, and ε, μ are the relative permittivity and permeability, respectively) is small compared to the wavelength in vacuum ($\lambda \sim c/\omega$), one cannot consider the field inside the conductor, but should write the boundary condition on its surface [2] as follows:

$$\mathbf{E}_\mathrm{t} = \sqrt{\frac{\mu\mu_0}{\varepsilon\varepsilon_0}}[\mathbf{H}_\mathrm{t}, \mathbf{n}], \qquad (1S)$$

where $\mathbf{E}_\mathrm{t}$ and $\mathbf{H}_\mathrm{t}$ is tangential components of electrical and magnetic field, respectively, μ_0 is vacuum permeability, ε_0 is vacuum permittivity, $\mathbf{n}$ is a vector normal to the surface. Note that for considered metals and the frequency range $\mu \approx 1$ and ε is a large complex value.

Value $\sqrt{\mu\mu_0/(\varepsilon\varepsilon_0)}$ is called the surface impedance of the metal ζ, which is inversely proportional to the complex refractive index $\sqrt{\varepsilon\mu} = n + \mathrm{i}k$ for non-magnetic materials. The impedance has a complex value that can be decomposed into the real and imaginary parts as $\zeta = \zeta' + \mathrm{i}\zeta''$. The losses in the waveguide are determined by the component of the Poynting vector normal to the waveguide wall that can be written as follows:

$$S_n = \frac{\zeta'}{2}|\mathbf{H}_\mathrm{t}|^2. \qquad (2S)$$

Thus, the losses depend on the real part of the surface impedance.

Note that this conclusion agrees with full modal analysis for straight (untapered) waveguides for moderately large $|n + \mathrm{i}k|$ [3]. For such waveguides a rigorous analysis of Gaussian beam propagation is also possible [4, 5], but it does not add significant insights in terms of power losses.

2. Polarization

The initial field at the entrance of the waveguide is a linearly polarized Gaussian beam [6], which can be decomposed into the sum of plane waves [2]. Changing the polarization of the beam as it passes through a waveguide can be qualitatively explained through the interference of these plane waves. The schematic representation of such interference is shown in Fig. S5.

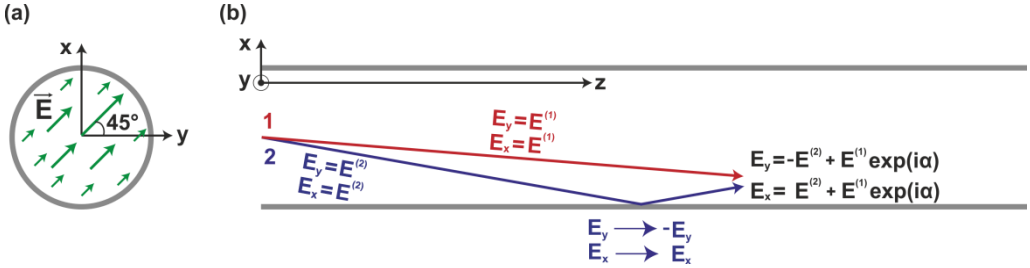

Fig. S5. (a) Position of the x- and y-axes relative to the direction of **E** of the incident beam. (b) Schematic representation of the interference of two plane waves propagating in a cross section coinciding with the xz-plane for a silver-coated waveguide. Wave 1 (red) travels to the point of interference without reflection, while wave 2 (blue) – with one reflection.

We consider a perfect metal (the limit of infinite ε or zero ζ) and propagation at small angles with respect to the waveguide axis (near grazing incidence at waveguide wall). Taking into account the interference of only two waves propagating in the xz-plane as it is shown in Fig. S5b, a field projection onto the x- and y-axes for the first wave can be written, respectively, as $E_x = E^{(1)}$ and $E_y = E^{(1)}$. Similarly, the second wave has projections $E_x = E^{(2)}$ and $E_y = E^{(2)}$, respectively.

The projections are equal, since in the considered cross section **E** has the same angle of 45° with both x- and y-axes. In the case of reflection of the wave 2 from the wall, the projection of the field onto the y-axis (s-polarization) changes sign, while the projection onto the x-axis (p-polarization) remains the same [2]. At the point of interference, the final projections onto the axes, taking into account that the waves receive a certain phase difference α (due to various path lengths) can be written as follows:

$$E_x = E^{(2)} + E^{(1)}e^{\mathrm{i}\alpha}, \quad (3S)$$

$$E_y = -E^{(2)} + E^{(1)}e^{\mathrm{i}\alpha}. \quad (4S)$$

The resulting projections have different amplitude and phases, implying the appearance of a general elliptical polarization. When many rays from different planes are combined, this leads to a complete loss of polarization at the output. Importantly, this holds even in paraxial case (when the rays only slightly deviate from the waveguide axis implying small values of α), if at least one reflection occurs in the waveguide (which changes sign of off-plane component). This is the drawback of metal-coated waveguides in comparison with dielectric ones.

By contrast, for hollow dielectric waveguides, the Fresnel amplitude reflection coefficients (r_p and r_s) strongly depend on the incidence angle [2]. They both approaches -1 for grazing angles, which is a desired property. The above interference is then still present, but it is the same for both x and y components and, thus, is independent of the specific field polarization in Fig. S5. Therefore, the original incidence polarization remains in the waveguide. Unfortunately, this property holds only for very small propagation angles (with respect to the waveguide axis). For $n = 2$ (typical for quartz in the THz range [7]) these coefficients increase to -0.7 and -0.9 already for 5°. Therefore, a hollow dielectric waveguide acts as a directional filter. The rays very close to the waveguide axis pass with small change of intensity and polarization, while other rays are both attenuated and depolarized. As a result, a typical Gaussian beam passing through this waveguide will lose significant energy but retain significant linear polarization.

The strong depolarization due to the metal coatings has also been discussed in ref. [4]. However, this qualitative discussion does not prove but only suggests that the transmitted wave will be depolarized by a metal-coated waveguide. The total polarization can be retained due to the problem symmetry – this was demonstrated by the rigorous modal analysis [5]. More specifically, the incident Gaussian beam can couple to the EH_{11} mode, which produces the linear polarized Gaussian beam at the output [8]. Similar result is obtained if several modes with almost equal propagation constants are involved – then they will interfere constructively at the output.

However, such polarization conservation can be expected only for untapered waveguides with highly conductive coating. First, EH_{11} and other linearly polarized modes correspond to non-paraxial rays, which are significantly affected by tapering. Second, for moderately conducting metals the Fresnel coefficient r_p (but not r_s) strongly depends on the incidence angle, similar to that for dielectric coating above. This coefficient rapidly changes from -1 for grazing incidence to almost 1 for angles several times larger than $1/|n + \mathrm{i}k|$ [4], but it does so over approximately circular trajectory in a complex plane. Thus $|r_\mathrm{p}|$ stays close to 1 in contrast to the case of dielectric coating. With increasing wavenumber in our range of interest the transition angle increases (due to decreasing $|n + \mathrm{i}k|$), while the Gaussian beam becomes less focused (for the same focus size) leading to smaller average incidence angle of constituent rays. When these two angles become comparable, part of the Gaussian beam is phase-shifted (and slightly attenuated) leading to loss of polarization. In other words, the above single-mode propagation is not possible anymore. For the largest considered wavenumber (1118 cm^{-1}) the third regime appears, when most of the constituent rays are in the grazing regime, with r_p close to -1 (similar to the case of the dielectric coating). This explains relatively larger degree of polarization for all metal and metal-coated waveguides at this wavenumber.

3. Computer parameters

System Manufacturer: ASUSTeK COMPUTER INC.
System Model: Z10PE-D16 Series
System Type: x64-based PC
Processor: Intel(R) Xeon(R) CPU E5-2620 v3 @ 2.40GHz, 2401 MHz, 6 Core(s), 12 Logical Processor(s).
Processor: Intel(R) Xeon(R) CPU E5-2620 v3 @ 2.40GHz, 2401 MHz, 6 Core(s), 12 Logical Processor(s).
BIOS Version: American Megatrends Inc. 0602, 05.02.2015
Type of Physical Memory: DDR4.
Total Physical Memory: 262 050 Mb
Available Physical Memory: 249 840 Mb
Virtual Memory: Max Size: 291 725 Mb
Virtual Memory: Available: 278 810 Mb

D. Photograph of the waveguides

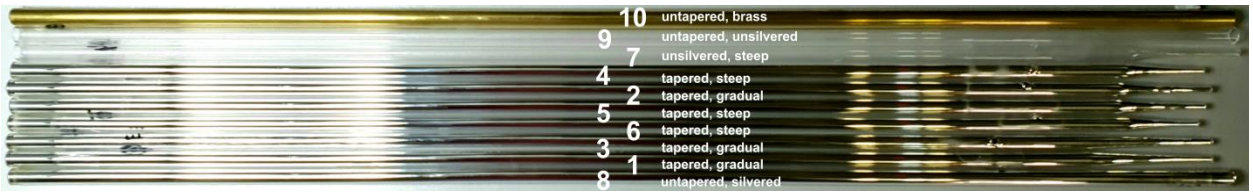

Fig. S6. Photograph of terahertz waveguides used in the work. The numbers and descriptions correspond to Table 1 of the main text.

E. References

[1] Kubarev V.V., Serednyakov S.S., The Measurement and Monitoring of Spectrum and Wavelength of Coherent Radiation at Novosibirsk Free Electron Laser, 10th International Workshop on Personal Computers and Particle Accelerator Controls, Karlsruhe, Germany, 2014, pp. 96-98.

[2] Landau L.D., Lifshits E.M., Electrodynamics of continuous media, by L. D. Landau and E. M. Lifshitz. Translated from the Russian by J. B. Sykes and J. S. Bell // Pergamon Press, Oxford – 1960. – 417 P.

[3] Marcatili E.A.J., Schmeltzer R.A. Hollow metallic and dielectric waveguides for long distance optical transmission and lasers // Bell Syst. Tech. J. – 1964. – Vol. 43. – №. 4. – P. 1783-1809. – 10.1002/j.1538-7305.1964.tb04108.x

[4] Crenn J.P. Gaussian beam transmission through circular waveguides with conducting wall material // Appl. Opt. – 1985. – Vol. 24. – №. 21. – P. 3648-3658. – 10.1364/AO.24.003648

[5] Gurin O.V., Degtyarev A.V., Maslov V.A., Svich V.A., Tkachenko V.M., Topkov A.N. Propagation of submillimetre laser beams in hollow waveguides // Quantum Electron. – 2005. – Vol. 35. – №. 2. – P. 175-179. – 10.1070/qe2005v035n02abeh002639

[6] Kubarev V.V., Sozinov G.I., Scheglov M.A., Vodopyanov A.V., Sidorov A.V., Melnikov A.R., Veber S.L. The Radiation Beamline of Novosibirsk Free-Electron Laser Facility Operating in Terahertz, Far-Infrared, and Mid-Infrared Ranges // IEEE T. THz Sci. Techn. – 2020. – Vol. 10. – №. 6. – P. 634-646. – 10.1109/TTHZ.2020.3010046

[7] Kitamura R., Pilon L., Jonasz M. Optical constants of silica glass from extreme ultraviolet to far infrared at near room temperature // Appl. Opt. – 2007. – Vol. 46. – №. 33. – P. 8118-8133. – 10.1364/AO.46.008118

[8] Crenn J.P. Optical study of the EH11 mode in a hollow circular oversized waveguide and Gaussian approximation of the far-field pattern // Appl. Opt. – 1984. – Vol. 23. – №. 19. – P. 3428-3433. – 10.1364/AO.23.003428